



# Mechanical strength of aneurysmatic and dissected human thoracic aortas at different shear loading modes



Gerhard Sommer<sup>a</sup>, Selda Sherifova<sup>a</sup>, Peter J. Oberwalder<sup>b</sup>, Otto E. Dapunt<sup>b</sup>,  
Patricia A. Ursomanno<sup>c</sup>, Abe DeAnda<sup>d</sup>, Boyce E. Griffith<sup>e</sup>, Gerhard A. Holzapfel<sup>a,\*</sup>

<sup>a</sup> Institute of Biomechanics, Graz University of Technology, Austria

<sup>b</sup> University Clinic of Cardiac Surgery, Medical University Graz, Austria

<sup>c</sup> Department of Cardiothoracic Surgery, NYU Langone Medical Center, New York, NY, USA

<sup>d</sup> Division of Cardiothoracic Surgery, University of Texas Medical Branch, Galveston, TX, USA

<sup>e</sup> Departments of Mathematics and Biomedical Engineering, University of North Carolina, Chapel Hill, NC, USA

## ARTICLE INFO

### Article history:

Accepted 21 February 2016

### Keywords:

Ultimate stress  
Thoracic aorta  
Aortic aneurysm  
Aortic dissection  
Connective tissue disorder

## ABSTRACT

Rupture of aneurysms and acute dissection of the thoracic aorta are life-threatening events which affect tens of thousands of people per year. The underlying mechanisms remain unclear and the aortic wall is known to lose its structural integrity, which in turn affects its mechanical response to the loading conditions. Hence, research on such aortic diseases is an important area in biomechanics. The present study investigates the mechanical properties of aneurysmatic and dissected human thoracic aortas via triaxial shear and uniaxial tensile testing with a focus on the former. In particular, ultimate stress values from triaxial shear tests in different orientations regarding the aorta's orthotropic microstructure, and from uniaxial tensile tests in radial, circumferential and longitudinal directions were determined. In total, 16 human thoracic aortas were investigated from which it is evident that the aortic media has much stronger resistance to rupture under 'out-of-plane' than under 'in-plane' shear loadings. Under different shear loadings the aortic tissues revealed anisotropic failure properties with higher ultimate shear stresses and amounts of shear in the longitudinal than in the circumferential direction. Furthermore, the aortic media decreased its tensile strength as follows: circumferential direction > longitudinal direction > radial direction. Anisotropic and nonlinear tissue properties are apparent from the experimental data. The results clearly showed interspecimen differences influenced by the anamnesis of the donors such as aortic diseases or connective tissue disorders, e.g., dissected specimens exhibited on average a markedly lower mechanical strength than aneurysmatic specimens. The rupture data based on the combination of triaxial shear and uniaxial extension testing are unique and build a good basis for developing a 3D failure criterion of diseased human thoracic aortic media. This is a step forward to more realistic modeling of mechanically induced tissue failure i.e. rupture of aneurysms or progression of aortic dissections.

© 2016 Elsevier Ltd. All rights reserved.

## 1. Introduction

Thoracic aortic aneurysms (TAAs) are localized dilatations of the ascending or descending thoracic aorta which develop over a span of years and may dissect (dissecting aneurysm) or rupture which is the most fatal condition. The mortality of thoracic aneurysms is estimated to be 50% over 5 years (Elefteriades, 2008), whereas the mortality of an untreated Type A dissection approaches 50% in the first 48 h. The pathogenesis of thoracic aneurysmal

\* Correspondence to: Institute of Biomechanics, Graz University of Technology, Stremayrgasse 16/II, 8010 Graz, Austria.

Tel.: +43 316 873 35500; fax: +43 316 873 35502.

E-mail address: [holzapfel@tugraz.at](mailto:holzapfel@tugraz.at) (G.A. Holzapfel).

<http://dx.doi.org/10.1016/j.jbiomech.2016.02.042>

0021-9290/© 2016 Elsevier Ltd. All rights reserved.

disease involves extracellular matrix degradation and loss of smooth muscle cells, causing a decrease in aortic wall integrity. The etiologies for these processes include atherosclerosis and genetic conditions such as Marfan's syndrome and Loey–Dietz syndrome (Elefteriades, 2008; Azadani et al., 2013). Hypertension has also been implicated as a cause.

Aortic dissection (AD) is an acute condition of the aorta which typically begins with a primary intimal tear on the right lateral wall of the ascending thoracic aorta (ATA), where the hydraulic shear force is at its peak, or at the descending thoracic aorta (DTA) directly after the ligamentum arteriosum (Kasper et al., 2015). The dissection first propagates in the radial direction towards the medial layer. Then, it proceeds within the media, or between the media and the adventitia, causing the layers of the aortic wall to

separate (Mikich, 2003). The separation allows the blood flow to enter the aortic wall, whereby a secondary channel, a so-called false lumen, is created. This leads to dilatation and weakening of the remaining outer wall of the false lumen which in turn increases the probability of the rupture and causes the patient to bleed to death within minutes (Oberwalder, 2001; Criado, 2011).

Interestingly, TAAs and ADs occur at similar locations in the thoracic aorta, presumably triggered by large hemodynamic forces and tissue stresses created in the left ventricular outflow tract when the heart contracts. Furthermore, the biomechanically important constituents of the elastic arterial wall are degraded during the process of the formation of TAA and AD. The main cause of TAA or AD is assumed to be hypertension, with an occurrence of 70%, and medial degeneration of the aorta (Isselbacher, 2005; Kasper et al., 2015). Rupture of the thoracic aorta is the main reason for morbidity and mortality of patients with Marfan's or Ehlers–Danlos syndromes (Kasper et al., 2015). Due to elevated cardiovascular stress, the appearance of a dissection or aneurysm increases with gestational age, i.e. it mostly occurs in older persons (> 50 years) (Oberwalder, 2001; Immer et al., 2003).

Considering the variety of reasons for developing thoracic aortic diseases, a better understanding of patient-specific biomechanical properties is essential for developing biomechanical markers to predict adverse events. Moreover, patient-specific biomechanics-based computational approaches which use wall stress and strength distributions will provide more reliable estimates of aneurysm rupture or aortic dissection initiation/progression (Vande Geest et al., 2006; Azadani et al., 2013). However, validation of biomechanics-based rupture indicators is needed before adaptation into the clinical paradigm.

A detailed analysis of the mechanical failure properties of aneurysmatic and dissected human thoracic aortas with a particular focus on four different shear tests is presented in this study. In particular, ultimate shear stresses and corresponding amount of shear values from mode II tests in four orientations, in addition to ultimate tensile stresses and corresponding stretch values from uniaxial tensile tests (in circumferential and longitudinal directions) and direct tension tests (in radial direction) of the aortic media, were determined.

2. Materials and methods

In the present study the media of diseased aortas (n=16; age: 58 ± 12 years) was investigated. The aortas were subdivided into three categories: 'aneurysmatic', 'aneurysmatic with connective tissue disorder (CTD)', and 'dissected'. In Table 1, the anamnesis of all donors from which the specimens were obtained are listed. Aneurysmatic specimens (n=9) are denoted as AI–AIX, aneurysmatic specimens

with CTD (n=3) are denoted as CI–CIII, and dissected specimens (n=4) are denoted as DI–DIV. More specifically, the donors of the CTD specimens had fibromyxoid degeneration (CI), MASS syndrome (CII), and Marfan's syndrome (CIII). Fibromyxoid degeneration is the transformation of fibrous tissue into a mucous-like 'connective' tissue characterized by the accumulation of glycosaminoglycans (O'Boynick et al., 1994). Marfan's syndrome is the result of a mutation in the FBN1 gene (gene for fibrillin-1) disrupting the elastic fiber assembly in the connective tissue by altering the regulation of TGF-β production (Dietz et al., 1991; Judge and Dietz, 2005), while MASS (mitral, aortic, skin, skeletal) syndrome, also the result of a mutation in the FBN1 gene, is very similar to Marfan's syndrome but with some differences in clinical manifestations (Judge and Dietz, 2005). In addition to the anamnesis, the aortic disease and the position where the specimens were harvested are provided.

Both dissected thoracic sections and unruptured TAA sections were obtained from consented patients undergoing surgical repair at the Department of Cardiothoracic Surgery, NYU Langone Medical Center, and the Department of Cardiac Surgery, Medical University of Graz, Austria. The study protocol and the use of material from human subjects were approved by the local Ethics Committee, Medical University of Graz, Austria. In Fig. 1(a) a typically obtained aneurysmatic tissue sample (CI) with a severely dilated diameter is presented.

2.1. Shear testing

Tubular aortic samples were cut along the longitudinal direction to obtain flat and rectangular sheets, and the media were separated with surgical tools. With the assumption of an orthotropic structure of the aortic tissue, the behavior under six possible shear modes are identified, i.e. two different shear properties in each of the three planes (Dokos et al., 2002; Sommer et al., 2015). Using cylindrical coordinates, these planes are referred to as the zθ-, rz- and rθ-planes (Fig. 2). We refer to the shear modes in the zθ-plane as 'in-plane' shear modes, and the shear modes regarding the rz- and rθ-planes as 'out-of-plane' shear modes, and emphasize that the 'out-of-plane' shear mode should not be confused with mode III fracture testing. In particular, 'in-plane' shear tests in the circumferential and longitudinal directions of the zθ-plane determine the ultimate shear stresses τ<sub>rθ</sub><sup>u</sup> and τ<sub>rz</sub><sup>u</sup>, respectively (Fig. 2(a)), whereas shearing in the radial and longitudinal directions of the rz-plane results in the 'out-of-plane' shear stress values τ<sub>θr</sub><sup>u</sup> and τ<sub>zr</sub><sup>u</sup>, respectively (Fig. 2(b)). In an analogous manner, 'out-of-plane' shear tests in the radial and circumferential directions of the rθ-plane result in the ultimate shear stresses τ<sub>zr</sub><sup>u</sup> and τ<sub>θr</sub><sup>u</sup>, respectively (Fig. 2(c)). Unfortunately, due to the restrictions arising from the specimen dimensions, we were only able to experimentally determine two out of four 'out-of-plane' shear stress values, τ<sub>θz</sub><sup>u</sup> and τ<sub>zθ</sub><sup>u</sup>.

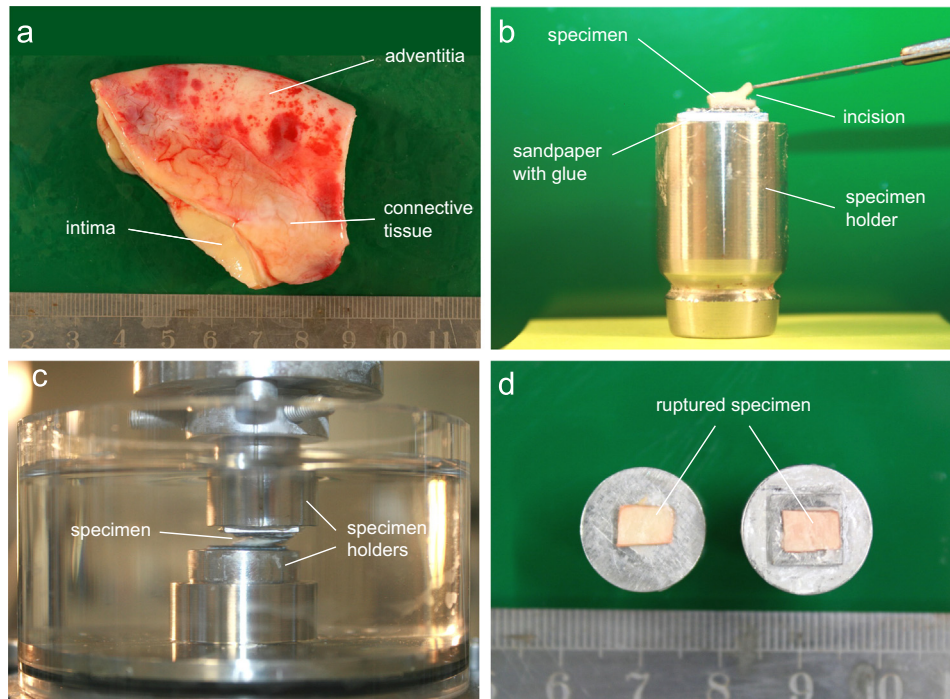
For 'in-plane' shear tests, small rectangular tissue samples with the dimensions of 5 mm in length and 4 mm in width were prepared. An incision of 1 mm in depth along the width of the specimen was introduced to induce a predetermined breaking point, leaving the area on which the load was applied by 4 × 4 mm (Figs. 1(b) and 3). Representative photographs during and after a successful 'in-plane' shear test are shown in Fig. 1(c) and (d), respectively. A special specimen geometry and preparation had to be developed to ensure failure of the tissue in the correct plane during 'out-of-plane' shear tests. A variety of specimen geometries were tested to obtain the 'out-of-plane' shear stress. The final working geometry of the specimen had the dimensions 8 × 3 mm (length × width) with non-symmetric incisions (dashed lines) from both sides on the long edge (Fig. 4). Sandpaper and a thin consistent layer of cyanoacrylate adhesive were used to fix the specimen between two cylindrical specimen holders (Sommer et al., 2013a, 2015). Additionally, a compressive force of 0.5 N was applied to the specimens for 5 min to ensure hardening of the adhesive and proper fixation of the specimen to the specimen holders. After 5 min of adhesive hardening, the compressive force was

Table 1

Donor information such as age, gender, connective tissue disorder (CTD), and risk factor are stated. Moreover, the condition of the aorta and the harvesting position are provided.

Donor information	Specimen denotation															
	AI	AII	AIII	AIV	AV	AVI	AVII	AVIII	AIX	CI	CII	CIII	DI	DII	DIII	DIV
Institute	MUG	MUG	NYU	MUG	NYU	NYU	NYU	NYU	MUG	MUG	NYU	NYU	NYU	MUG	MUG	MUG
Age, yr	71	71	64	50	72	62	43	50	66	56	52	28	43	65	58	73
Gender	M	M	M	M	F	M	M	M	M	F	M	F	M	M	M	M
Condition	AN	AN	AN	AN	AN	AN	AN	AN	AN	AN	AN	AN	DI	DI	DI	DI
Position	ATA	ATA	ATA	ATA	ATA	ATA	ATA	ATA	ATA	ATA	ATA	DTA	DTA	ATA	ATA	ATA
CTD	–	–	–	–	–	–	–	–	–	FD	MA	MF	–	–	–	–
Risk factors	HT	HT	HT	HT	HT	AS	AR	AS	HT	HT	HT	HT	HT	HT	HT	HT
		HL	HL	HL	HL	HM			HL	SM	HL		SM			DM
				OB					SM		OB					

AN, aneurysmatic; AR, aortic regurgitation; AS, atherosclerosis; ATA, ascending thoracic aorta; DI, dissected; DM, diabetes mellitus; DTA, descending thoracic aorta; F, female; FD, fibromyxoid degeneration; HM, heart murmur; HL, hyperlipidemia; HT, hypertension; M, male; MA, MASS syndrome; MF, Marfan's syndrome; MUG, Medical University Graz; NYU, New York University; OB, obesity; SM, smoker.



**Fig. 1.** (a) Representative photograph of a human ascending aortic aneurysm sample (CI) with a severely dilated diameter; (b) typical specimen with an incision of  $\sim 1$  mm for in-plane shear testing, which is glued to the upper specimen holder before insertion in the testing apparatus; (c) photograph of an 'in-plane' specimen subjected to simple shear loading; (d) ruptured into two parts and successfully tested 'in-plane' specimen.

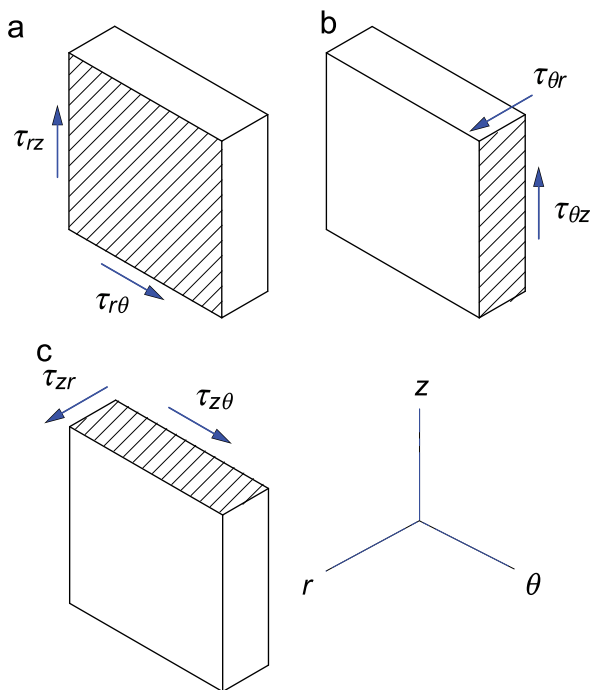


**Fig. 2.** Sketches of six shear modes defined with respect to the radial ( $r$ -axis), circumferential ( $\theta$ -axis), and longitudinal ( $z$ -axis) direction on an orthotropic tissue piece. Arrows indicate shear directions with corresponding shear stresses  $\tau_{ij}$  and  $i, j \in \{r, \theta, z\}$ , where  $i$  denotes the normal vector of the plane that is being sheared, and  $j$  denotes the direction in which the face is shifted. For example, (a) shows 'in-plane'-shear modes in the  $z\theta$ -plane with shear in  $z$ - and  $\theta$ -directions, while (b) and (c) show 'out-of-plane'-shear modes in the  $rz$ - and  $r\theta$ -plane, respectively.

reduced to 0 N, and the actual shear test was started. During testing, the lower platform moved relative to the fixed upper platform with a constant speed of 1 mm/min. The applied force that led to failure was defined as the shear failure

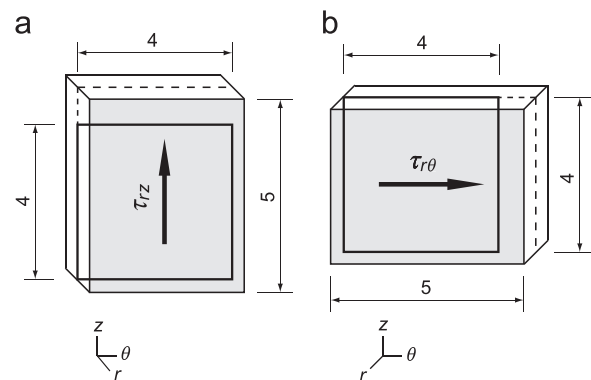


**Fig. 3.** Sketches of 'in-plane' shear test specimens in the longitudinal direction ( $rz$ -mode), (a), and in the circumferential direction ( $r\theta$ -mode), (b), to obtain shear properties of the  $z\theta$ -plane. The shaded surfaces are glued to the specimen holders and sheared. The specimen is longer in the direction in which it is being sheared ( $\sim 5$  mm). On the shorter edge an incision of 1 mm parallel to the shearing direction is introduced (dashed lines). The remaining area (thick-lined black rectangular) is sheared until rupture occurs. Arrows indicate the shear directions.

force. The 'amount of shear' was calculated as the ratio of the relative in-plane displacement of two parallel plates to their separation distance. The shear stress  $\tau$  was calculated as the shear force  $f$  divided by the sheared area  $a$ .

## 2.2. Uniaxial tensile testing

In addition to shear tests, uniaxial tensile rupture tests in the radial, circumferential and longitudinal directions were conducted. For the determination of the radial failure stress, direct tension tests were performed with cylindrical specimens ( $\varnothing 6.0$  mm) with an incision of  $\sim 1.0$  mm around the circumference until failure. For more details the reader is referred to Sommer et al. (2008). For uniaxial tensile tests until rupture in the circumferential and longitudinal directions, dog-bone-shaped specimens were elongated until failure. For more details about specimen geometry, testing protocol and setup see Sommer et al. (2013b).

All tests, except direct tension tests, were performed with the specimens inside a perspex container filled with PBS solution, which was maintained at a constant

temperature of 37 °C (Sommer et al., 2013a,b, 2015). Upon completion of the individual tests, each sample was inspected regarding the penetration of glue along its unattached sides.

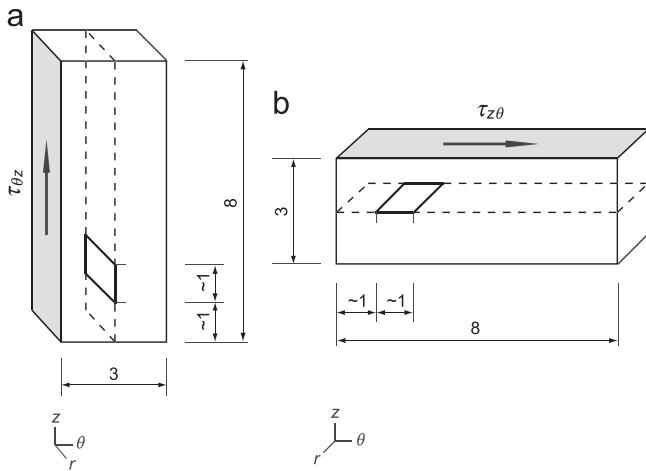


**Fig. 4.** Sketches of 'out-of-plane' shear test specimens: (a) shear properties in the  $rz$ -plane; (b) shear properties in the  $r\theta$ -plane obtained from these tests. The shaded surfaces are glued to the specimen holders of the apparatus and sheared. The specimen is longer in the direction in which it is being sheared (8 mm). On the shorter edge (3 mm), incisions parallel to the shearing direction are introduced from both sides (dashed lines). The thick-lined black parallelogram between the incised surfaces is the sheared surface, with the dimension of  $\sim 1$  mm, parallel to the longer edge. Arrows indicate the shear directions.

### 2.2.1. Microstructural investigation

Second-harmonic generation (SHG) imaging of 'in-plane' and 'out-of-plane' tests in the circumferential direction of specimen AIX was performed after mechanical testing, and after optical clearing following the procedure in Schrieff et al. (2013).

### 2.3. Statistical analyses

Statistical analyses were performed to test for significant differences of the mechanical stress values between different orientations and shear testing modes, i.e. between ultimate shear stresses and stretches in the circumferential and longitudinal directions, and between 'in-plane' and 'out-of-plane' shearing using paired two-sample  $t$ -test.  $p$ -values were determined based on Student's  $t$ -distribution, where  $p < 0.05$  was considered to be significant. Statistical analyses were performed using the OriginLab ORIGIN 7.5 program package. All data values are presented as mean values (mean)  $\pm$  standard deviation (SD).

## 3. Results

In total, 16 diseased human thoracic aortas – 9 aneurysmatic, 3 aneurysmatic with CTD and 4 dissected – were investigated in this study.

### 3.1. Ultimate shear stress from 'in-plane' and 'out-of-plane' testing

'In-plane' shear stress vs. amount of shear behavior of successfully tested specimens in the circumferential ( $r\theta$ -mode) and longitudinal directions ( $rz$ -mode) obtained from aneurysmatic tissues and aneurysmatic tissues with CTD are shown in Fig. 5.

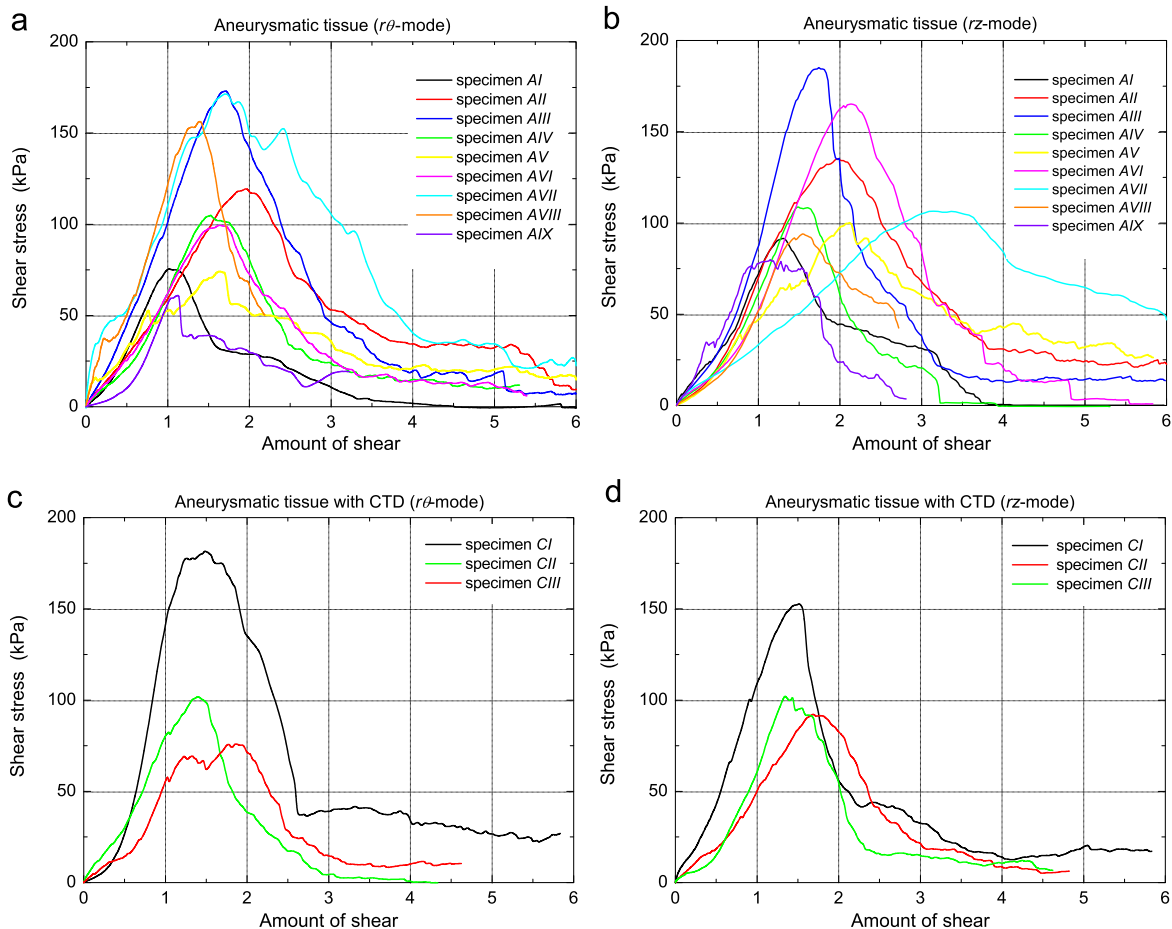


**Fig. 5.** Cauchy shear stress vs. amount of shear relationship during 'in-plane' shear tests of aneurysmatic human thoracic aortic tissues: (a), (b) 'in-plane' shear behavior within the  $r\theta$ - and  $rz$ -modes of aneurysmatic tissues, respectively; (c), (d) 'in-plane' shear behavior within the  $r\theta$ - and  $rz$ -modes of aneurysmatic tissues with connective tissue disorders (CTD), respectively.

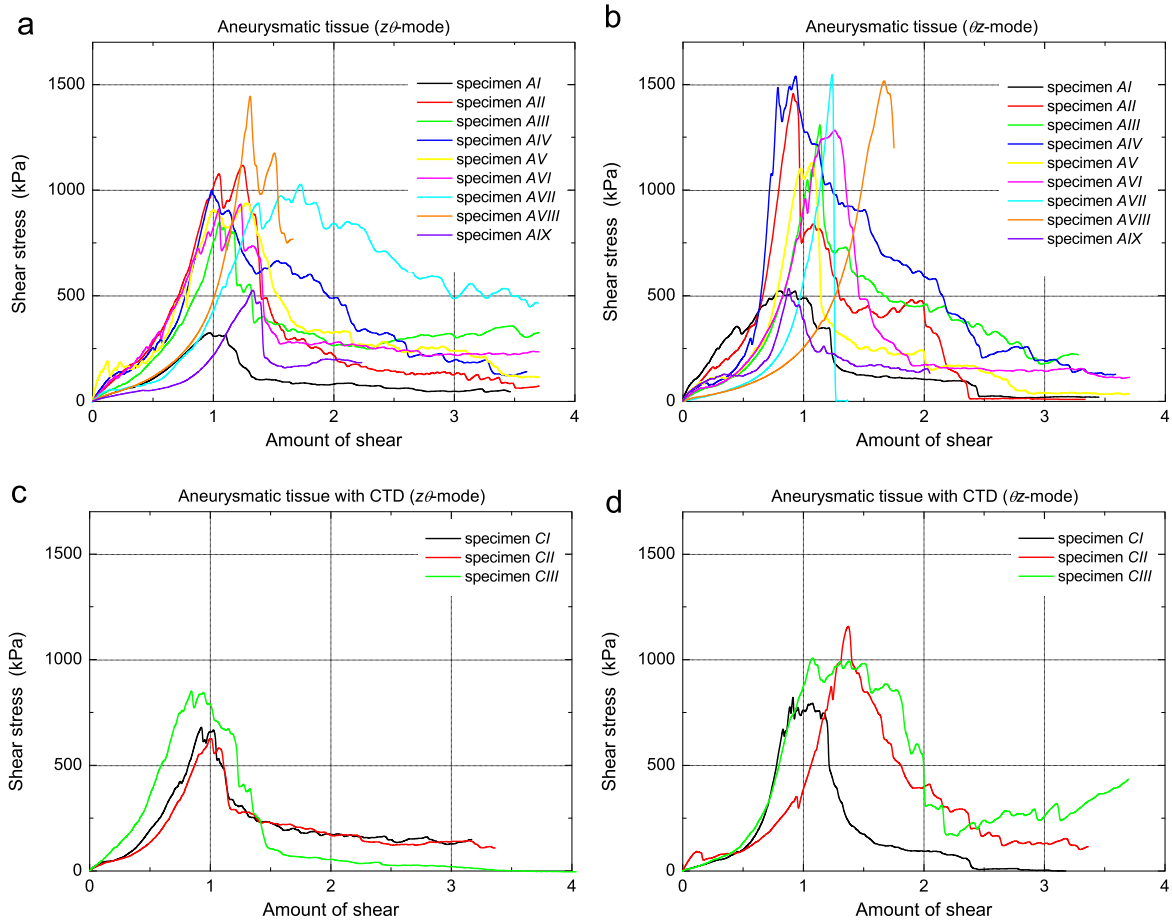


**Fig. 6.** Cauchy shear stress vs. amount of shear relationship during ‘out-of-plane’ shear tests of aneurysmatic human thoracic aortic tissues: (a), (b) ‘out-of-plane’ shear behavior of aneurysmatic tissues within the  $z\theta$ - and  $\theta z$ -modes, respectively; (c), (d) ‘out-of-plane’ shear behavior of aneurysmatic tissues with connective tissue disorders (CTD), respectively.

**Table 2**

Ultimate shear stress  $\tau^u$  and corresponding amount of shear  $\gamma^u$  for aneurysmatic specimens subjected to ‘in-plane’ shear within the  $r\theta$ - and  $rz$ -modes, and ‘out-of-plane’ shear within the  $z\theta$ - and  $\theta z$ -modes.

Specimen	‘In-plane’ shear				‘Out-of-plane’ shear			
	$\tau_{r\theta}^u$ (kPa)	$\gamma_{r\theta}^u$	$\tau_{rz}^u$ (kPa)	$\gamma_{rz}^u$	$\tau_{z\theta}^u$ (kPa)	$\gamma_{z\theta}^u$	$\tau_{\theta z}^u$ (kPa)	$\gamma_{\theta z}^u$
AI	76	1.02	92	1.30	325	0.97	528	0.94
AII	120	1.97	135	1.98	1122	1.24	1467	0.92
AIII	105	1.53	109	1.49	860	1.05	1349	1.14
AIV	173	1.71	185	1.74	1011	0.99	1563	0.79
AV	74	1.63	100	2.12	946	1.27	1138	1.08
AVI	100	1.63	165	2.13	947	1.23	1292	1.26
AVII	173	1.73	106	3.14	1035	1.74	1565	1.24
AVIII	157	1.40	94	1.55	1479	1.31	1529	1.67
AIX	61	1.12	80	1.15	533	1.33	548	0.88
Mean	115	1.53	118	1.84	918	1.24	1221	1.10
SD	41	0.28	34	0.56	313	0.22	388	0.25

Corresponding results of the ‘out-of-plane’ shear tests in the circumferential ( $z\theta$ -mode) and longitudinal ( $\theta z$ -mode) directions of all aneurysmatic tissues and aneurysmatic tissues with CTD are given in Fig. 6. In Tables 2 and 3, ultimate shear stresses and corresponding amount of shear values obtained from ‘in-plane’ and ‘out-of-plane’ shear tests of aneurysmatic and aneurysmatic with CTD are listed. Moreover, ‘in-plane’ shear responses in the circumferential ( $r\theta$ -mode) and longitudinal ( $rz$ -mode) directions of dissected specimens are given in Fig. 7. Unfortunately, due to

**Table 3**

Ultimate failure shear stress  $\tau^u$  and corresponding amount of shear  $\gamma^u$  for aneurysmatic tissues with CTD subjected to ‘in-plane’ shear within the  $r\theta$ - and  $rz$ -modes, and ‘out-of-plane’ shear within the  $z\theta$ - and  $\theta z$ -modes.

Specimen	‘In-plane’ shear				‘Out-of-plane’ shear			
	$\tau_{r\theta}^u$ (kPa)	$\gamma_{r\theta}^u$	$\tau_{rz}^u$ (kPa)	$\gamma_{rz}^u$	$\tau_{z\theta}^u$ (kPa)	$\gamma_{z\theta}^u$	$\tau_{\theta z}^u$ (kPa)	$\gamma_{\theta z}^u$
CI	182	1.48	153	1.52	688	0.93	836	0.92
CII	102	1.40	92	1.69	629	1.00	1163	1.38
CIII	76	1.85	103	1.35	859	0.84	1011	1.08
Mean	120	1.58	116	1.52	725	0.92	1003	1.13
SD	45	0.20	27	0.14	98	0.07	134	0.19

the small specimen size ‘out-of-plane’ shear tests for dissected specimens could not be performed. Table 4 states the ultimate shear stresses and corresponding amount of shear values from ‘in-plane’ tests of the dissected thoracic aortas. Interestingly, most tissue specimens from the AI–AIX and DI–DIV groups (except AVII and AVIII) revealed higher ultimate shear stresses in the longitudinal direction when compared with the circumferential direction under ‘in-plane’ shear loading (Tables 2–4). Similarly, all specimens showed higher ultimate stresses in the longitudinal than in the circumferential direction under ‘out-of-plane’ shear loading (Tables 2 and 3).

In comparison with ‘in-plane’ shear tests, ‘out-of-plane’ shear tests exhibited much higher ultimate shear stress values.

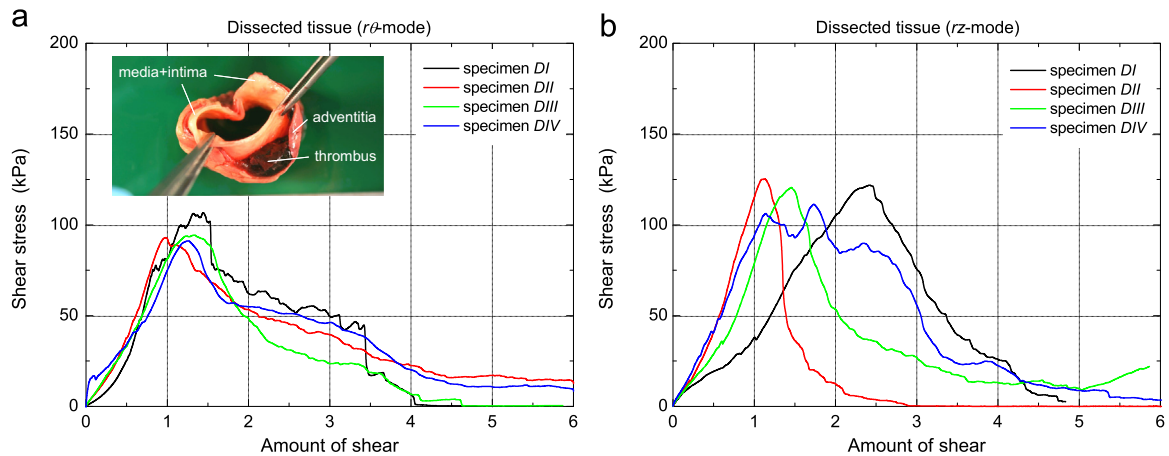


**Fig. 7.** Cauchy shear stress vs. amount of shear relationship during 'in-plane' shear tests of dissected human thoracic aortic tissues: (a), (b) in the  $r\theta$ - and  $rz$ -modes, respectively.

**Table 4**

Ultimate shear stress  $\tau^u$  and corresponding amount of shear  $\gamma^u$  for dissected specimens subjected to 'in-plane' shear within the  $r\theta$ - and  $rz$ -modes.

Specimen	'in-plane' shear			
	$\tau_{r\theta}^u$ (kPa)	$\gamma_{r\theta}^u$	$\tau_{rz}^u$ (kPa)	$\gamma_{rz}^u$
DI	107	1.45	122	2.42
DII	93	0.98	126	1.13
DIII	95	1.33	121	1.46
DIV	91	1.27	111	1.74
Mean	97	1.26	120	1.69
SD	6	0.17	6	0.47

Consequently, aortic tissues indicate a much higher resistance to rupture subjected to 'out-of-plane' shear loading than 'in-plane' shear loading.

### 3.2. Ultimate tensile stress in radial, circumferential, and longitudinal directions

A characteristic behavior in all radial tests could be observed (not shown herein). During direct tension tests in the radial direction, the tissue showed an elastic behavior at small displacements represented by an ascending steep slope (nonlinear stiffening). After an 'elastic limit' was reached, a second phase, a strongly nonlinear softening behavior, started where damage and micro-defects gradually occurred. After reaching the maximal force (radial failure force) a third phase started, where the tissue dissected until complete tissue failure, which was very similar to the behavior observed in Sommer et al. (2008). The average ultimate tensile stress and stretch of the samples ( $n=13$ ) were determined to be  $\bar{\sigma}_r^u = 131 \pm 56$  kPa and  $\bar{\lambda}_r^u = 2.66 \pm 0.68$ , respectively.

Average ultimate tensile stresses and corresponding stretches in the circumferential and longitudinal directions were determined to be  $\bar{\sigma}_{\theta\theta}^u = 1282 \pm 822$  kPa,  $\bar{\lambda}_{\theta}^u = 1.52 \pm 0.20$  ( $n=7$ ) and  $\bar{\sigma}_{zz}^u = 565 \pm 198$  kPa,  $\bar{\lambda}_z^u = 1.50 \pm 0.18$  ( $n=10$ ), respectively. These values indicate anisotropic mechanical failure properties, with preferably higher mechanical strength in the circumferential than in the longitudinal direction. This anisotropic behavior may be explained by the preferred collagen fiber alignment in the circumferential direction of the thoracic aortic media (Schriebl et al., 2012).

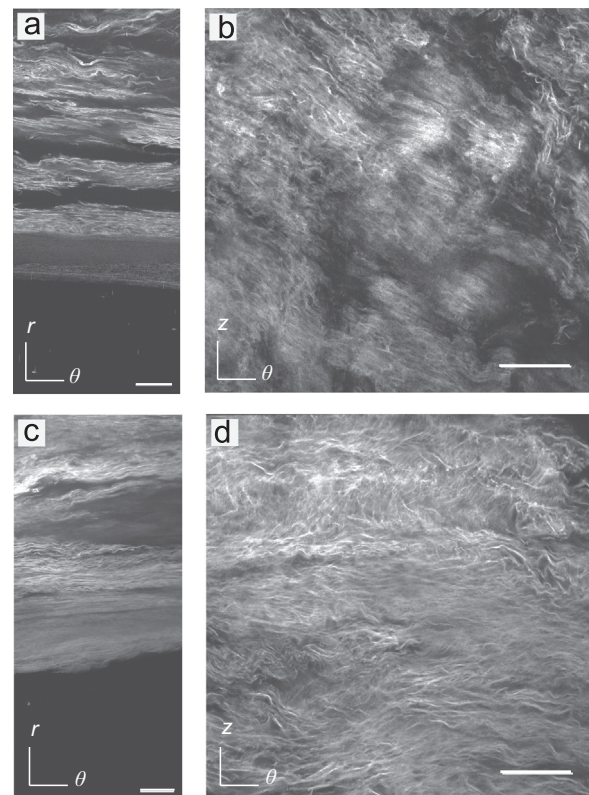


**Fig. 8.** Representative SHG images of specimen AIX showing the collagen architecture: (a), (c) images taken from the  $r\theta$ -plane and (b), (d) images from the  $z\theta$ -plane of shear test samples in circumferential direction. Panels (a), (b) represent the planes normal and parallel to the plane of shearing of an 'in-plane' test sample, respectively; panels (c), (d) represent the planes parallel and normal to the shearing plane of an 'out-of-plane' test sample, respectively. White bars indicate 100  $\mu\text{m}$ .

### 3.3. Microstructural investigation

Representative SHG images of sample AIX are shown in Fig. 8. Panels (a) and (b) show the collagen architecture in the  $r\theta$ - and  $z\theta$ -planes of the 'in-plane' shear test in the circumferential direction, respectively, while panels (c) and (d) show the collagen architecture in  $r\theta$ - and  $z\theta$ -planes of the 'out-of-plane' shear test in the circumferential direction, respectively. Images in panels (b) and (c) are parallel, whereas panels (a) and (d) are normal to the planes being sheared in 'in-plane' and 'out-of-plane' shear tests.

#### 4. Discussion

The present study investigates the mechanical strength of diseased human thoracic aortas with respect to its anisotropic structure, with a particular emphasis on the shear properties. It is required to obtain relevant mechanical data of human thoracic aortas to better understand which type of stresses are responsible for inducing a crack and how this crack is propagating in the arterial wall to study rupture of diseased walls and propagation of aortic dissections more deeply. Furthermore, such data are prerequisites for the development of a failure criterion in thoracic aortic tissues, or for the design of better aortic grafts. To the authors' knowledge, this is the first investigation of the failure properties of diseased human thoracic aortic tissues under combined simple shear and uniaxial extension loadings.

*Shear testing:* 'In-plane' shear tests revealed anisotropic failure properties of thoracic aortic tissue with slightly higher ultimate shear stresses ( $p=0.44$ ) and significantly higher amounts of shear ( $p=0.02$ ) in the longitudinal than in the circumferential direction. Interestingly, ultimate 'in-plane' shear stresses in the circumferential and longitudinal directions were not significantly different for aneurysmatic tissues ( $p=0.84$ ), but significantly different for dissected tissues ( $p=0.009$ ). However, this trend was not observed for the corresponding amount of shear values ( $p > 0.07$ ). Similar to 'in-plane' shearing, 'out-of-plane' shear tests showed significant anisotropic failure properties with higher ultimate shear stresses in the longitudinal than in the circumferential direction ( $p=0.0003$ ), but with not significantly different amounts of shear ( $p=0.57$ ) (see also Tables 2–4). Remarkably, the aortic media revealed approximately one order of magnitude higher ultimate shear stress values for 'out-of-plane' loading than for 'in-plane' loading ( $p < 0.0001$ ) with significantly smaller amounts of shear for 'out-of-plane' loading than 'in-plane' loading ( $p < 0.006$ ). Consequently, under mixed shear loading state, the tissue will most likely fail due to 'in-plane' shearing and not due to 'out-of-plane' shearing. Furthermore, we observed several 'peaks' in the shear stress vs. amount of shear plots obtained from 'out-of-plane' tests, as can be seen in Fig. 6, which did not occur during 'in-plane' shear tests (see Fig. 5). This behavior may be attributed to the irregular rupture of collagen fibers and their interconnections.

Collagen fibers are the main load bearing structures in the arterial wall at large deformation and are known to be responsible for the high strength of arterial tissues subjected to tensile and shear loading. The elastin network in the media, including elastic lamellae, interlamellar elastin fibers, and radial elastin struts, certainly contribute to the shear properties at small deformation. However, the contribution of the elastin network to the shear strength behavior is small since failure occurs at large deformation. Moreover, for aneurysmatic and dissected tissues the contribution of the elastin network is very small, because elastin is usually disintegrated in such diseased tissues. Studies on aortic aneurysmatic tissues by, e.g., Tong et al. (2013), revealed a very low elastin contents in the abdominal aortic aneurysms due to pathological changes and remodeling. The collagen architecture, visualized by second-harmonic generation (SHG) imaging (Fig. 8), suggests that the large difference in the ultimate shear stresses may be related to the collagen fiber orientation and dispersion. From Fig. 8 one can appreciate that the collagen fibers embedded within the parallel planes to the plane of shearing have only little resistance to shear displacements. In other words, fibers embedded in the  $z\theta$ -plane hardly contribute to the resistance of the specimen which is being sheared in the  $z\theta$ -plane ('in-plane' testing modes). However, this is an idealization of the real structure. One should consider that the collagen fibers embedded in these parallel planes are interconnected by, e.g., proteoglycans, smooth muscle cells, and remaining elastin network, which might also

contribute to the shear strength. Furthermore, the dispersed fibers connecting these parallel planes create a resistance in the planes normal to the plane of shearing. For example, out-of-plane fiber dispersion will resist shear displacement under 'in-plane' testing. We expect that the resistance to shearing, hence the shear strength, to be correlated with the mean fiber direction and the in plane dispersion of the fibers in the case of 'out-of-plane' testing, and with the out-of-plane fiber dispersion in the case of 'in-plane' testing (for the definitions of mean fiber direction and fiber dispersion see Holzapfel et al., 2015).

Recently Haslach et al. (2015) also performed shear tests on rectangular blocks, but on bovine aortas, which correspond to 'in-plane' shear in the present paper. In line with our findings, they reported no significant differences in stresses between the longitudinal and circumferential directions. Furthermore, they observed voids in the histology of test samples in the plane normal to the applied shear which is also evident in Fig. 8(a). Since their testing protocol and reporting method are different, we are not able to make a direct comparison with shear stress and amount of shear values that we have obtained. To identify the shear modulus (ratio between shear stress and amount of shear) inflation–extension–torsion tests were performed on human common carotid arteries (Kas'yanov et al., 1978), on rat thoracic aortas (Deng et al., 1994), and on porcine coronary arteries (Lu et al., 2003). All these studies showed that the shear modulus was constant with changing twist angle while the longitudinal stretch and the inner pressure were kept constant at chosen physiological levels. Furthermore, the shear modulus was different for different values of longitudinal stretch and applied internal pressure (Kas'yanov et al., 1978; Lu et al., 2003), and the relation became nonlinear at pressure levels higher than 120 mmHg (Kas'yanov et al., 1978). The maximum twist angle applied in these studies was  $25^\circ$  under a mixed loading state. The experimental curves indicated in the present study, both 'in-plane' and 'out-of-plane', also showed linearity at low amount of shear, but with a larger variability, as evident from Fig. 5. Interestingly, the study (Kas'yanov et al., 1978) stated that at twist angles of  $70$ – $80^\circ$  the tubular specimens lost their resistance. The maximum amount of shear ( $\gamma_{rz} = 3.14$ , sample AVII) in our study corresponds approximately to  $72^\circ$  shearing of a rectangular sample. However, we cannot make direct comparisons since the authors did not report any failure values. To the authors' knowledge, comparable data in which shear loadings lead to failure of arterial tissues are not available in the literature.

*Uniaxial tensile testing:* In comparison with existing data, the average radial failure stress of the diseased human thoracic aortic media ( $\bar{\sigma}_r^u = 131 \pm 56$  kPa ( $n=13$ )) was slightly higher than that of the human carotid bifurcations ( $124 \pm 25$  kPa ( $n=25$ )) (Tong et al., 2011), and it was very similar to the average radial failure stress of aged healthy human abdominal aortic medias ( $140.1 \pm 15.9$  kPa ( $n=8$ )) (Sommer et al., 2008).

The average radial failure stresses of the diseased thoracic aortic media were significantly lower than corresponding stresses in the circumferential ( $\bar{\sigma}_{\theta\theta}^u = 1282 \pm 822$  kPa ( $n=7$ )) ( $p < 0.001$ ) and longitudinal directions ( $\bar{\sigma}_{zz}^u = 565 \pm 198$  kPa ( $n=10$ )) ( $p < 0.001$ ), which may be explained by the laminar organization of the media with collagen fibers preferably found in the circumferential–longitudinal plane. Ultimate tensile stresses in the circumferential direction were on average significantly higher (about twice as high) than the ultimate stresses in the longitudinal direction ( $p=0.03$ ), which reflects pronounced anisotropic behavior. This anisotropy may be explained by the orientation of embedded collagen fibers, which are preferably orientated in the circumferential direction (Schriebl et al., 2012). In contrast, the study of Vorp et al. (2003) found similar ultimate tensile stresses in the circumferential ( $1180 \pm 120$  kPa ( $n=23$ )) and longitudinal directions ( $1210 \pm 90$  kPa ( $n=17$ )) of thoracic aortic aneurysms.

However, a more recent study (Pichamuthu et al., 2013) revealed, on average, very similar ultimate tensile stresses in thoracic aortic aneurysms to our study ( $1309 \pm 80$  kPa ( $n=38$ ) in the circumferential direction and  $619 \pm 34$  kPa ( $n=38$ ) in the longitudinal direction).

Interestingly, ultimate stretches in the radial direction ( $\bar{\lambda}_r^u = 2.66 \pm 0.68$  ( $n=13$ )) were significantly higher than ultimate stretches in the circumferential ( $\bar{\lambda}_\theta^u = 1.52 \pm 0.20$  ( $n=7$ )) ( $p < 0.001$ ) and longitudinal directions ( $\bar{\lambda}_z^u = 1.50 \pm 0.18$  ( $n=10$ )) ( $p < 0.001$ ). Average ultimate stretches in the circumferential and longitudinal directions were not significantly different ( $p=0.85$ ). However in the literature, failure stretches in the circumferential and longitudinal directions of thoracic aortic aneurysms were determined to be different ( $1.95 \pm 0.05$  vs.  $1.55 \pm 0.03$ ) (Pichamuthu et al., 2013).

Moreover, we found correlations between the mechanical properties of the tested aortic tissues and the anamnesis of the patients. For example, it is interesting how ultimate stresses differ with respect to the underlying disease (aneurysm, tissue disorder, or dissection). Dissected specimens exhibited on average a markedly lower mechanical strength, than aneurysmatic specimens. Similarly, aneurysmatic specimens from donors suffering from connective tissue disorders showed distinctly lower ultimate stress values than other aneurysmatic specimens. This may reflect the risk of patients with connective tissues disorders developing or suffering from aneurysms. The variability in the mechanical strength of the aneurysmatic samples may be attributed to different stages of aneurysms.

**Limitations:** Due to the small specimen size it was not always possible to conduct all tests on every specimen. This is the reason for not presenting 'out-of-plane' shear data for dissected specimens. Tissues with pronounced inhomogeneities such as atherosclerotic plaques were unsuitable for this investigation, resulting in the reduction of the amount of tissue available for testing, and hence in a reduced specimen number. Furthermore, a large number of uniaxial tension tests (in circumferential or longitudinal directions) failed because the rupture occurred near one of the clamps instead of the gage region. When there was adequate tissue material available, however, a second specimen was prepared and tested. SHG through the thickness of sample A1X revealed that there were thin intimal-like collagen fibers on one end, and thick adventitial-like collagen fibers at the other end of the image stack. Even though the layers could be easily peeled off in several cases, the borderlines between the intima/media and media/adventitia, especially for aneurysmatic samples, were not always clearly visible due to the process of aneurysm formation. For more discussion on that issue see Niestrawska et al. (2016). All tests were conducted with an extension rate of 1.0 mm/min, although it is not established that this rate corresponds to a physiological value. However, there are no data available at which speed a dissection or rupture propagates in the case of an *in vivo* situation. The small amount of dissected and connective tissue disorder samples may lead to inadequate statistically relevant results. This also presents an obstacle to draw further meaningful conclusions.

Nevertheless, for the first time, this study presents methodologies for investigating biomechanical rupture properties of soft biological tissues in the context of different failure modes. Furthermore, the rupture data based on the combination of triaxial shear and uniaxial extension testing data are unique and build a good information basis for developing a 3D failure criterion of the diseased human thoracic aortic media; taking us a step closer to a realistic modeling of mechanically induced tissue failure.

#### Conflict of interest statement

None declared.

#### Acknowledgments

The authors are indebted to Anju R. Babu, Florian Hartmann, Gabrijela Korica, Franz Seiringer, and David Walk for their valuable contributions to the experimental tests and structural investigations. We would like to thank Annette E. Rabinovich for her valuable support during tissue transportation. Furthermore, we gratefully acknowledge the financial support of the National Institutes of Health (NIH), research Grant no. NIH R01HL117063.

#### References

- Azadani, A.N., Chitsaz, S., Mannion, A., Mookhoek, A., Wisneski, A., Guccione, J.M., et al., 2013. Biomechanical Properties of Human Ascending Thoracic Aortic Aneurysms. *Ann. Thorac. Surg.* 96, 50–58.
- Criado, F.J., 2011. Aortic dissection: a 250-year perspective. *Tex. Heart Inst. J.* 38, 694–700.
- Deng, S.X., Tomioka, J., Debes, J.C., Fung, Y.C., 1994. New experiments on shear modulus of elasticity of arteries. *Am. J. Physiol. Heart Circ. Physiol.* 266, H1–H10.
- Dietz, H.C., Cutting, G.R., Pyeritz, R.E., Maslen, C.L., Sakai, L.Y., Corson, G.M., et al., 1991. Marfan syndrome caused by a recurrent de novo missense mutation in the fibrillin gene. *Nature* 352, 337–339.
- Dokos, S., Smail, B.H., Young, A.A., LeGrice, I.J., 2002. Shear properties of passive ventricular myocardium. *Am. J. Physiol.* 283, H2650–H2659.
- Elefteriades, J.A., 2008. Thoracic aortic aneurysm: reading enemy's playbook. *Yale J. Biol. Med.* 81, 175–186.
- Haslach Jr., H.W., Leahy, L.N., Fathi, P., Barrett, J.M., Heyes, A.E., Dumsha, T.A., et al., 2015. Crack propagation and its shear mechanisms in the bovine descending aorta. *Cardiovasc. Eng. Technol.* 6, 501–518.
- Holzappel, G.A., Niestrawska, J.A., Ogden, R.W., Reinisch, A.J., Schriefl, A.J., 2015. Modelling non-symmetric collagen fibre dispersion in arterial walls. *J. R. Soc. Interface* 12, 20150188.
- Immer, F.F., Bansi, A.G., Immer-Bansi, A.S., McDougall, J., Zehr, K.J., Schaff, H.V., et al., 2003. Aortic dissection in pregnancy: analysis of risk factors and outcome. *Ann. Thorac. Surg.* 76, 309–314.
- Isselbacher, E.M., 2005. Thoracic and abdominal aortic aneurysms. *Circulation* 111, 816–828.
- Judge, D.P., Dietz, H.C., 2005. Marfan's syndrome. *Lancet* 366, 1965–1976.
- Kasper, D.L., Fauci, A.S., Longo, D.L., Hauser, S.L., Jameson, J.L., Loscalzo, J., 2015. Harrison's Principle of Internal Medicine, 19th ed. McGraw-Hill Professional, New York.
- Kas'yanov, V.A., Purinya, B.A., Tseders, ÉÉ., 1978. Determination of the shear modulus of human blood-vessel walls. *Polym. Mech.* 14, 753–755.
- Lu, X., Yang, J., Zhao, J.B., Gregersen, H., Kassab, G.S., 2003. Shear modulus of porcine coronary artery: contributions of media and adventitia. *Am. J. Physiol. Heart Circ. Physiol.* 285, 1966–1975.
- Mikich, B., 2003. Dissection of the aorta: a new approach. *Heart* 89, 6–8.
- Niestrawska, J.A., Viertler, C., Regitnig, P., Cohnert, T.U., Sommer, G., Holzappel, G.A., 2016. Mechanics and microstructure of healthy and aneurysmatic abdominal aortas: experimental analysis and modeling. Submitted for publication.
- Oberwalder, P.J., 2001. Aneurysmen und Dissektionen der thorakalen Aorten: Definition und Pathologie. *J. Kardiol.* 8, 2–4.
- O'Boynick, P., Green, K.D., Batnitzky, S., Kepes, J.J., Pietak, R., 1994. Aneurysm of the left middle cerebral artery caused by myxoid degeneration of the vessel wall. *Stroke* 25, 2283–2286.
- Pichamuthu, J.E., Phillippi, J.A., Cleary, D.A., Chew, D.W., Hempel, J., Vorp, D.A., et al., 2013. Differential tensile strength and collagen composition in ascending aortic aneurysms by aortic valve phenotype. *Ann. Thorac. Surg.* 96, 2147–2154.
- Schriefl, A.J., Wolinski, H., Regitnig, P., Kohlwein, S.D., Holzappel, G.A., 2013. An automated approach for 3D quantification of fibrillar structures in optically cleared soft biological tissues. *J. R. Soc. Interface* 10, 20120760.
- Schriefl, A.J., Zeindlinger, G., Pierce, D.M., Regitnig, P., Holzappel, G.A., 2012. Determination of the layer-specific distributed collagen fiber orientations in human thoracic and abdominal aortas and common iliac arteries. *J. R. Soc. Interface* 9, 1275–1286.
- Sommer, G., Gasser, T.C., Regitnig, P., Auer, M., Holzappel, G.A., 2008. Dissection of the human aortic media: an experimental study. *J. Biomech. Eng.* 130 021007–1–12.
- Sommer, G., Eder, M., Kovacs, L., Pathak, H., Bonitz, L., Mueller, C., et al., 2013a. Multiaxial mechanical properties and constitutive modeling of human adipose tissue: a basis for preoperative simulations in plastic and reconstructive surgery. *Acta Biomater.* 9, 9036–9048.
- Sommer, G., Schriefl, A., Zeindlinger, G., Katzensteiner, A., Ainödhofner, H., Saxena, A., et al., 2013b. Multiaxial mechanical response and constitutive modeling of esophageal tissues: impact on esophageal tissue engineering. *Acta Biomater.* 9, 9091–9379.
- Sommer, G., Schriefl, A.J., Andrä, M., Sacherer, M., Viertler, C., Wolinski, H., et al., 2015. Biomechanical properties and microstructure of human ventricular myocardium. *Acta Biomater.* 24, 172–192.

- Tong, J., Cohnert, T., Regitnig, P., Holzapfel, G.A., 2011. Effects of age on the elastic properties of the intraluminal thrombus and the thrombus-covered wall in abdominal aortic aneurysms: biaxial extension behavior and material modeling. *Eur. J. Vasc. Endovasc. Surg.* 42, 207–219.
- Tong, J., Schriefl, A.J., Cohnert, T., Holzapfel, G.A., 2013. Gender differences in biomechanical properties, thrombus age, mass fraction and clinical factors of abdominal aortic aneurysms. *Eur. J. Vasc. Endovasc. Surg.* 45, 364–372.
- Vande Geest, J.P., Wang, D.H.J., Wisniewski, S.R., Makaroun, M.S., Vorp, D.A., 2006. Towards a noninvasive method for determination of patient-specific wall strength distribution in abdominal aortic aneurysms. *Ann. Biomed. Eng.* 34, 1098–1106.
- Vorp, D.A., Schiro, B.J., Ehrlich, M.P., Juvonen, T.S., Ergin, M.A., Griffith, B.P., 2003. Effect of aneurysm on the tensile strength and biomechanical behavior of the ascending thoracic aorta. *Ann. Thorac. Surg.* 80, 1210–1214.